Particle-in-Cell simulation of radio-frequency ion thruster RIT-1.0

Ninad Joshi[1,2]* and Christian Heiliger[1,2]

*Correspondence:
ninad.joshi@theo.physik.uni-giessen.de

[1] Institute for Theoretical Physics, Justus-Liebig-University Giessen, Heinrich-Buff-Ring 16, Giessen 35392, Hessen, Germany
[2] Zentrum fuer Materialforschung, Justus-Libieg-University Giessen, Heinrich-Buff-Ring 16, Giessen 35392, Hessen, Germany

Abstract

Ion propulsion systems with a small thrust can be used in space missions for highly accurate controllability while possessing low power and propellant consumption. At the University of Giessen, radio-frequency ion thrusters are miniaturized with thrusts in the order of micro-Newtons (μN-RIT). As the size of the thruster becomes smaller the plasma properties can not be measured inside a closed plasma chamber. The simulations are needed to investigate plasma properties like temperature, density profile which would aid further opimization. In this work, we discuss kinetic simulations of plasma inside the RIT-1.0 thruster using in-house developed *PlasmaPIC* code that incorporates Monte-Carlo collisions (MCC) and Direct Simulation Monte Carlo (DSMC) for neutral gas distribution. We briefly present the features of *PlasmaPIC* and simulation of stable plasma generation. We also show the influence of neutral gas and extraction properties for the RIT-1.0 thruster under consideration.

Keywords: Particle-in-Cell, Kinetic modelling, Plasma simulation, Ion thruster

Introduction

At the University of Giessen, inductively coupled ion sources were adapted as a thruster for spacecraft propulsion systems [1]. Radio-frequency ion thrusters (RIT) generate the thrust by ejecting ions with a high velocity of up to 30 km/s [2, 3]. This type uses an inductive plasma discharge, which is the key to the extremely long lifetime [4]. Featured with an extraction grid system for accelerating the ions enables a high specific impulse for good efficiency. In the past years, the RIT was miniaturized with a diameter in the range of a few centimetres leading to thrusts on the order of micro-Newtons (μN-RIT), which are needed for ultra-fine positioning of the spacecraft [5–7]. As a matter of fact, the μN-RIT fulfils the requirements of a wide range of controllable thrust with high precision [8, 9]. RIT-1.0 is the smallest version of the radio-frequency ion thruster family to be developed at the University of Giessen with a diameter of 1 cm. The geometry of RIT-1.0 is based upon the RIT-2.5 which was built and characterized for its performance. A scaled down version with the diameter reduced by a factor of 2.5 is proposed as a next possible miniature thruster. Due to its small size, it is very difficult to diagnose the plasma properties inside the thruster chamber using any experimental setup. Hence, simulations for plasma parameters are necessary to investigate the plasma and

the thruster functioning. Since one cannot measure the plasma properties like density or temperature dependent on input power and gas flow, simulation is the only way to estimate the stability of plasma inside such small structure. These simulations are also interesting for research group working in different fields dealing with plasmas in small chamber [10]. In inductively coupled plasmas, at low pressures, when the electron mean free path is comparable to the discharge size, kinetic effects come into play, and the electron distribution function can be substantially non-Maxwellian. Therefore, a particle-based simulation tool is preferred for the understanding of plasma properties. Moreover, the typical neutral gas pressure in this thruster is in the order of 0.1 Pa. As a consequence validity of fluid dynamics is not guaranteed and standard commercial tools cannot be used. In the further sections, we describe the Particle-in Cell method, modelling of the RIT-1.0 plasma, and the performance issues required to be addressed for thruster construction.

PlasmaPIC: a Particle-in-Cell simulation code

For the simulation of ion thrusters multiple codes are developed by different research groups those are optimized for particular research interests. Our house developed simulation code, named *PlasmaPIC*, is a versatile code developed to simulated different types of plasmas e.g. inductively or capacitively coupled plasmas, discharge tube, ion beam transport for material interactions. The code is also intended to support the other groups involved in research of complex (dusty) plasmas and material research within the University. It has been validated by comparing results with well known XOOPIC code as a part of a doctoral thesis [11, 12]. In this framework, it was optimized to predict plasma properties induced by electromagnetic induction in the ion thruster using Particle-in-Cell (PIC) method [13, 14]. Along with the Monte Carlo Collision method, a full three-dimensional kinetic description of plasma inside a small discharge chamber can be investigated. The plasma properties are thus simulated using the "ab initio" -style, incorporating basic processes and conditions which may influence the composition of the plasma with a given set of input parameters.

A single computational cycle of the PIC algorithm consists of particle mover, interpolation of charge and current source terms to the grid, computation of the fields on the grid points and finally interpolation of the fields from the grid to the particle locations [15]. Figure 1 depicts the PIC scheme describing a computational cycle.

The initialization of the phase-space of particles can be implemented by assuming a predefined distribution of particles or a more generalized Monte Carlo collision method is used as in *PlasmaPIC*. The ions and electrons are produced by implementing power deposition from an external RF coil, which leads to the collection of charged and neutral particles or in other words the ignited plasma with background neutral gas.

Monte-Carlo Collisions

The Monte Carlo Collision (MCC) using the "null-collision" method is implemented in *PlasmaPIC* [16]. The MCC method assumes a neutral background gas in the volume of interest with a known density distribution. For the electron-neutral interaction, three types of collisions are considered namely the elastic scattering, the excitation, and the ionization. Given the high mass and velocity difference of the colliding partners, the
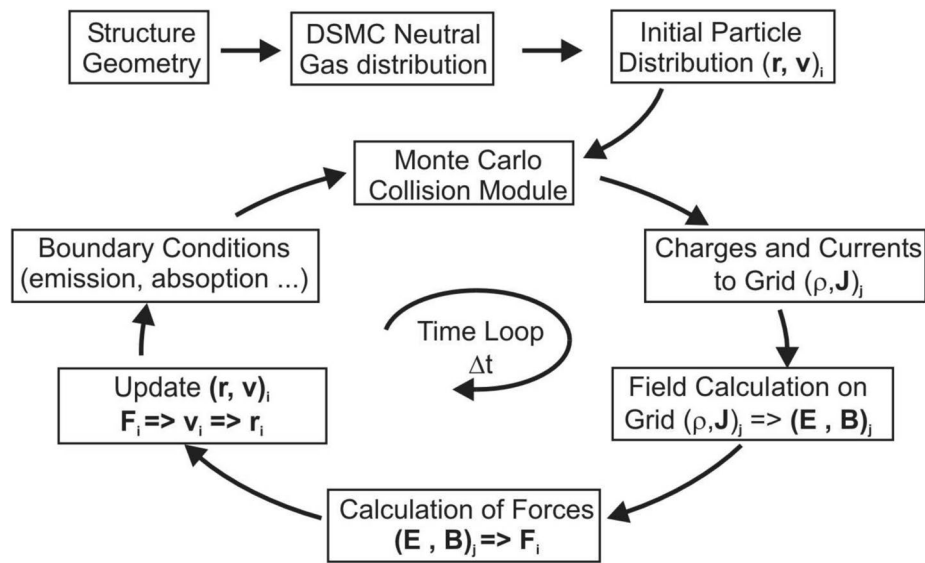
Fig. 1 Particle-in-Cell scheme describing a computational cycle

neutral particle is assumed to be stationary. In the event of ionization, a new electron and a new ion are created by the incident electron. The velocity of the new ion is randomly chosen assuming a Maxwellian distribution with a given temperature of the neutral gas. The energy of the incident electron is reduced by the ionization energy and has to be partitioned between the incident and the newly created electron. For the ion-neutral collision, only the elastic collisions are considered in *PlasmaPIC*. For the collision test, the relative velocity of the ion and the neutral particle has to be calculated. Because the neutrals are considered as a background density, the velocity of a pseudo gas particle has to be created using a Maxwellian distribution. Assuming the hard-sphere model the collision can be described by a uniform and isotropic scattering in the centre of mass frame. The special type of elastic scattering, the charge exchange, is treated separately. In this context, the newly created velocity is assigned to the ion, reflecting the fact that the neutral acquires a positive charge to become an ion.

Charge distribution

A first-order weighting scheme is used to assign the charge to grid points. For numerical stability, certain conditions need to be satisfied. The size of the time step depends on the largest frequency in the simulation. Commonly, this is the electron plasma frequency. For a minimum numerical error, the grid size should resolve the Debye length to describe the particle-particle interaction by the grid quantities accurately. The ratio of super-particles to real particles determines the number of super-particles in a cell or the number of particles in the Debye sphere.

Field calculation

For the modelling of an inductively coupled plasma, as in a RIT, a common approach is to separate Maxwell equations into an electrostatic and an electrodynamic part [17–20].

The electrical fields from both parts are then superimposed. For the electrostatic part the Poisson equation

$$\nabla^2 \phi = -\frac{\rho}{\epsilon_0} \tag{1}$$

is solved in every time step, where ϕ is the potential and ρ the charge. Dirichlet boundary conditions are incorporated as initial conditions. The interaction of charged particles and the plasma-wall effects (plasma sheath) is taken care of in this electrostatic part. The solution on the grid is obtained by an iterative method, which will be discussed in Elliptic equation solvers section.

The electrodynamic part is solved using the inhomogeneous wave equation also known as the Telegrapher's equation

$$\nabla^2 - \mu_0 \epsilon_0 \frac{\partial^2}{\partial t^2} \mathbf{E}(\mathbf{r}, t) = \mu_0 \frac{\partial}{\partial t} \mathbf{j}(\mathbf{r}, t), \tag{2}$$

where $\mathbf{E}(\mathbf{r}, t)$ and $\mathbf{j}(\mathbf{r}, t)$ are the time-varying electric fields and currents at grid points. The Telegraphers equation assumes charge neutrality, which is true in this case except for the sheath region. But it can be neglected as it is comparably small. By assuming harmonically varying fields and currents, one can represent them in complex form as

$$\mathbf{E}(\mathbf{r}, t) = \tilde{\mathbf{E}}(\mathbf{r})e^{i\omega t}, \tag{3}$$

$$\mathbf{B}(\mathbf{r}, t) = \tilde{\mathbf{B}}(\mathbf{r})e^{i\omega t}, \tag{4}$$

$$\mathbf{j}(\mathbf{r}, t) = \tilde{\mathbf{j}}(\mathbf{r})e^{i\omega t}, \tag{5}$$

where ω is the applied frequency. The time-dependent part can be separated into

$$\left(\nabla^2 + \mu_0 \epsilon_0 \omega^2\right)\mathbf{E}(\mathbf{r}, t) = i\omega \mathbf{j}(\mathbf{r}, t). \tag{6}$$

The total current $\mathbf{j}(\mathbf{r})$ is composed of the coil current $\mathbf{j}(\mathbf{r})_{coil}$ and electron current $\mathbf{j}(\mathbf{r})_{electron}$ in the plasma. The current due to ions is neglected due to their low mobility. The complex magnetic field amplitude is determined by

$$\mathbf{B}(\mathbf{r}, t) = \frac{i}{\omega}\nabla \times \mathbf{E}(\mathbf{r}, t). \tag{7}$$

Elliptic equation solvers

The finite-difference method is used to solve the Poisson equation. The Poisson equation is discretized to give potential ϕ at mesh position i, j, k by,

$$\phi_{i,j,k} = \frac{\Delta x^2 \rho_{i,j,k}}{6\epsilon_0} + \frac{1}{6}\Big(\phi_{i-1,j,k} + \phi_{i+1,j,k} +$$
$$+ \phi_{i,j-1,k} + \phi_{i,j-1,k} + \phi_{i,j,k-1} + \phi_{i,j,k+1}\Big), \tag{8}$$

where we use a uniform rectangular mesh with the same inter-node spacing Δx in each dimension i, j, k.

In *PlasmaPIC* the Successive Over Relaxation (SOR) algorithm is used for small structures [21]. In the SOR algorithm, the red-black scheme is implemented. $\phi_{i,j,k}^{m}$ of the current iteration step m is mixed with $\phi_{i,j,k}^{m-1}$ from the earlier iteration step,

$$\phi_{i,j,k}^{m} = (1 - \Omega)\phi_{i,j,k}^{m-1} + \Omega\phi_{i,j,k}^{m}. \tag{9}$$

Ω is called the relaxation parameter.

Geometry representation

PlasmaPIC can handle any arbitrarily shaped 3D objects. These objects are exported in STL format using a standard Computer-Aided Design (CAD) tool e.g. Gmsh. The surface of every object is represented by triangles, only objects with a volume are allowed. The triangles are imported into the geometry-module of the *PlasmaPIC* and consequently mapped on the cells of the simulation grid, which are occupied by the object. By marking these cells the object is reproduced in sugar-cube structure in *PlasmaPIC*. That way the shape of the object is cornered. Unfortunately, the surface is represented stepwise and hence the smoothness of the surface is lost. Nevertheless, this method drastically reduces the computational effort and the function needs to be called only once at the beginning.

PlasmaPIC currently supports the following objects with different properties,

- *Dielectric*: A dielectric object is an insulator. Once an electron or ion strikes the surface the particle sticks at that position of the surface. Therefore, this position of the surface can be charged by these particles. For every dielectric object, a specific permittivity is considered and can be defined by the user.
- *Equipotential*: This class of objects has a fixed potential that cannot be altered. So the particles will be removed once they strike these objects without charging the object. It is assumed that any quantity of current can drain off instantaneously. This treatment corresponds to an ideal voltage source.
- *Plasma region*: By importing a geometry consisting of different objects the area containing plasma is not defined. For this reason, an additional object is needed. All cells occupied by the plasma region object are the only ones allowed to hold the plasma.

Integration of the equations of motion

The motion of particles in the presence of electric and magnetic field is given by,

$$m\frac{d\mathbf{v}}{dt} = q(\mathbf{E} + \mathbf{v} \times \mathbf{B}) \tag{10}$$

where the quantities $\mathbf{E}$ and $\mathbf{B}$ are interpolated at particle positions from grid points. The "Boris Pusher" is used, which decouples electric and magnetic forces, achieving second-order accuracy by taking average velocities as,

$$m\frac{\mathbf{v}_{new} - \mathbf{v}_{old}}{dt} = q\left(\mathbf{E} + \frac{\mathbf{v}_{new} + \mathbf{v}_{old}}{2} \times \mathbf{B}\right). \tag{11}$$

By defining,

$$\mathbf{v}_{old} = \mathbf{v}^- - \frac{q\mathbf{E}}{m}\frac{\Delta t}{2}, \tag{12}$$

$$\mathbf{v}_{new} = \mathbf{v}^+ + \frac{q\mathbf{E}}{m}\frac{\Delta t}{2} \tag{13}$$

leads to

$$\frac{\mathbf{v}^+ - \mathbf{v}^-}{\Delta t} = \frac{q}{2m}\left(\mathbf{v}^+ + \mathbf{v}^-\right) \times \mathbf{B}. \tag{14}$$

In this formalism, a particle with the velocity $\mathbf{v}_{old}$ of the last time step is accelerated by the electric field for a half-time step leading to an interim velocity $\mathbf{v}^-$ of the particle. This interim velocity $\mathbf{v}^-$ is rotated by the magnetic field and a new interim velocity $\mathbf{v}^+$ is obtained. Finally, the particle is accelerated again by the electric field leading to the new velocity $\mathbf{v}_{new}$ of the particle for the single time step. The Boris method is known for its long time accuracy [22].

Direct simulation Monte Carlo module

For the modelling of the neutral gas distribution with reduced particle-particle interactions, the Direct Simulation Monte Carlo (DSMC) method is well suited [23]. The algorithm was developed by Bird and is used widely in many simulation packages [24]. It can also be applied for molecular flow without losing accuracy but it is computationally wasteful for this task. The DSMC is similar to the PIC algorithm described earlier. As in a PIC algorithm, the particles are represented by super-particles and space as well as time are discretized. The main differences between PIC and DSMC are the absence of electromagnetic forces and the particle-wall collisions. The velocity of a particle in DSMC is changed in particle-particle or particle-wall collisions only. The No Time Counter method is used for a reduced number of operations [25]. DSMC module can also be used independently as a stand-alone simulation tool, known as *FlowSim* [26]. Using the DSMC module the neutral gas density distribution can be initialized for MCC simulation instead of predefined homogenous or Maxwellian distribution for a more realistic scenario. In the following work though, the DSMC model is not used and homogeneous gas distribution is assumed due to time step constraints.

Extraction and ion beam diagnosis

The extraction module is used to simulate ion beam formation or the plume formation downstream of the thruster. Since the extraction electrodes are too thin compared to the chamber, a separate simulation domain with a higher spatial resolution in the longitudinal direction is required. In the current scenario, this module is only activated, once stable conditions of the plasma are reached. The extraction module is written in both cartesian and cylindrical coordinate systems. Although the cylindrical coordinate system

is fully three-dimensional using (r, θ, z) coordinates, it is efficient in the cases with cylindrical symmetry e.g. extraction orifice at centre or ring electrodes.

The diagnostics module defined as kind of a collector downstream of a thruster records the position and momentum of extracted particles. With this module, one can investigate exhaust plumes and correlate them with the plasma properties. The beam emittance is defined in terms of the area occupied by particles in phase-space.

$$\epsilon_x = \int \int dx \, dx' \tag{15}$$

More precisely, the rms-emittance is used to study the behaviour of an ion distribution. In $x - x'$, it is defined as

$$\tilde{\epsilon}_x = \left(\overline{x^2} \, \overline{x'^2} - (\overline{xx'})^2 \right)^{1/2}. \tag{16}$$

From transversal emittance, the plasma temperature can be estimated. The diagnostics module also delivers the extraction current and energy. The histogram of the particle population can be then used to investigate the energy distribution of the extracted ions or the neutral particle passing through the extraction orifice.

Parallelization

A PIC plasma simulation demands a huge amount of computational power. For example, the Poisson equation has to be solved for vast meshes of the size $100 \times 100 \times 100$ and larger. Millions of particles have to be accelerated for a couple of million time steps. For this purpose, Message Parsing Interface (MPI) is incorporated in *PlasmaPIC*. The domain decomposition method divides the total simulation space into subspaces and each subspace is assigned to a single thread. These threads only have to communicate boundary information of their subspaces with their six neighbours. The extraction module is separately activated and communication is managed through MPI's grouping algorithm.

3D modelling of μ-RIT-1.0

μN-RIT-1.0 (or simply RIT-1.0) has a diameter of 1 cm and the height is in the same range. The RIT-1.0 geometry is shown in Fig. 2. The coil (red) is wrapped in 5 loops around the discharge chamber (grey) starting with a radius of 6 mm, which decreases from a certain height to follow the dome-shaped discharge chamber thus keeping the distance from vessel constant at 1 mm. The thruster is completed by two grids (dark grey). Each grid has a thickness of 2 mm and the grid-gap is 8 mm. At the inner grid, a voltage of 1500 V is applied whereas the outer grid is set to -150 V.

The simulation domain is restricted to the plasma region alone, ignoring the extraction region or the exhaust plume. All particles that strike the exit plane (black - filling the aperture of the inner grid) contribute to the extraction current and will be stored for consecutive extraction simulation. For simulation singly charged Xenon ions (Xe^+) with mass 131.29 AMU was used with electrons. The electron and Xenon ion densities are initialized with a homogeneous distribution of $2.5 \times 10^{16}/\text{m}^3$. Xenon is used as a working neutral gas with a density of $8.5 \times 10^{19}/\text{m}^3$. The numerical
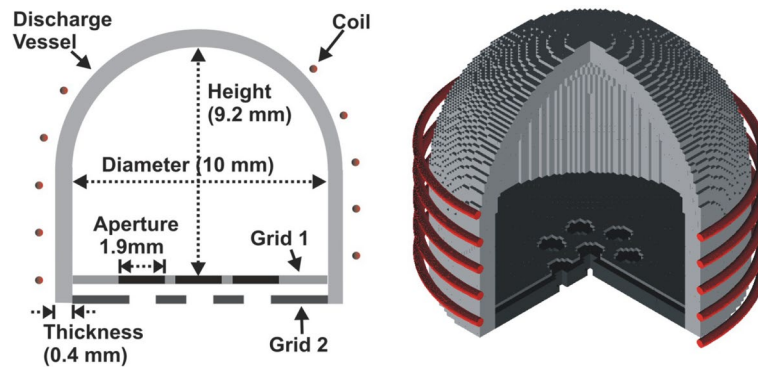
Fig. 2 A scheme of RIT-1.0 and the sugar-cube model generated in *PlasmaPIC* by importing CAD model. (colour on-line)

parameters are as follows: a cell size of 0.11 mm, a time step of 5×10^{-12} s, and a super-particle ratio of 1000. This leads to around $100 \times 100 \times 100$ cells and ten million electrons and ions, that have to be processed. The Debye length corresponds to about 0.088 mm and plasma frequency 8.91×10^9 Hz, thus satisfying Hockney and Eastwood condition [13], given by

$$\Delta x < 3.4\lambda_D,$$
$$\Delta t < 2\omega_{pe}^{-1}, \tag{17}$$

and also resolves the the applied rf-frequency of 5 MHz. The simulation was executed over nine million time steps corresponding to 45 μs, or 225 rf-cycles.

Figure 3 shows the snapshots of the temporal evolution of ion density in the discharge vessel. Figure 3a and b show the forming of the sheath and pre-sheath. In each rf-cycle, the coil current is slowly increased to avoid any dramatic increase in the plasma density leading to numerical instabilities. Figure 3c-f show the rise in the ion density with slowly increasing power deposition until the maximum value is reached. From Fig. 3g to k, it can be seen that the almost rotationally symmetric ion density distribution changes to a non-symmetric one. On the left side, a high-density area of ions is formed that stays constant until the end of the simulation. This highly irregular density distribution is due to two factors; first the coil is not rotationally symmetric because of the slope and second the decreasing radius at the curved top of the thruster. By substituting the coil with five single loops (see Sensitivity of the design section Fig. 9) the rotationally symmetric ion density can achieved.

As seen in Fig. 4 the coil current is slowly increased and the power is deposited in the system. The number of particles drops down initially but slowly increases to a stable value with the number of ions little more than the number of electrons. The mean energy of the ions also reaches a stable value but the electron energy oscillates around a stable average value.

Figure 5 shows an enlarged view of Fig. 4. Since the electric field accelerates and decelerates the electrons twice in each rf-cycle changing the wall potential, the electron temperature fluctuates with a frequency of 10 MHz, which is twice the applied frequency of the coil current (5 MHz). As the Xenon ion is much heavier the variation
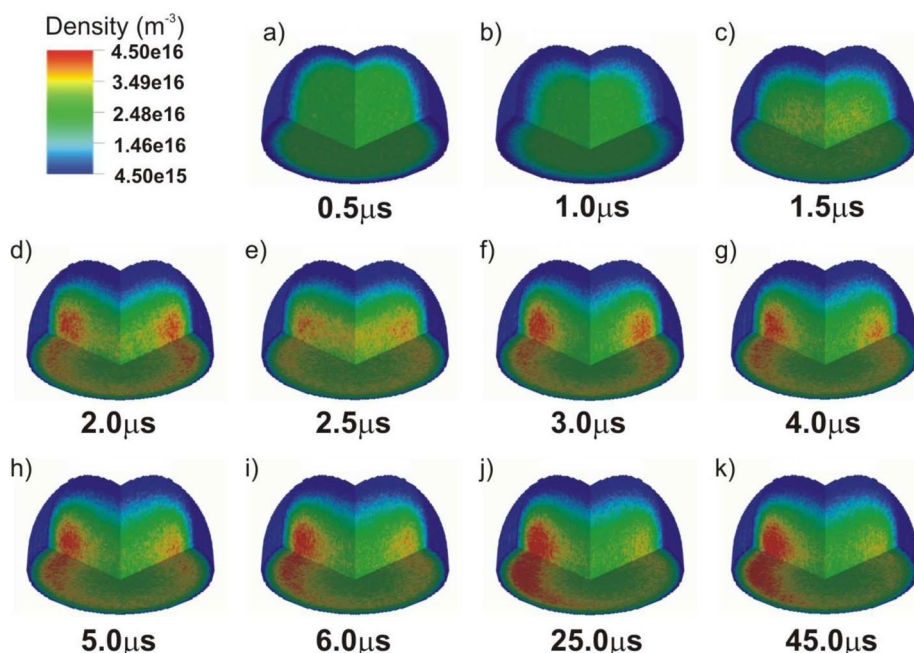
Fig. 3 Temporal evolution of ion density over the period of 45 μs with snapshots at selected timeframe. (colour on-line)

in ion temperature is much smaller than the variation in electron temperature as observed from the plot.

Figure 6 shows the probability density function (PDF) for electrons at the minimum point and the maximum point of the energy after achieving stable plasma conditions. From the analytical calculation assuming $E_{min} = 7.68$ eV and $E_{max} = 10.65$ eV, it can seen that the PDF follows the analytical curve up to $E = 20$ eV in the case of lower energy region and up to $E = 30$ eV at the higher energy region. After these values, the simulated PDF vastly deviates from the theoretical Maxwell-Boltzmann distribution. The main reason for this is the smaller size of the chamber, which influences plasma potential distribution from bulk to the plasma sheath.

Figure 7 shows the variation of extracted current and transversal emittance as a function of power deposition. The extraction current is proportional to the power deposition. As a consequence, the plasma density has to rise by the same factor. The transversal emittance on the other hand has minima at $P = 0.06$ Watt. This indicates a matched case of extraction for the chosen grid geometry at these values.

Influence of background neutral gas

In general, one assumes the plasma density in the discharge chamber to be the highest value in the middle and falling down radially. However, from the simulation, it is shown that the plasma density distribution depends on the neutral gas pressure in the discharge chamber. Although we can not confirm this from experiments, a qualitative comparison can be done.

Schaefer measured the radial plasma density distribution as a function of the neutral gas pressure in RIT-10 (diameter $= 10$ cm) [27]. Figure 8c shows density plots
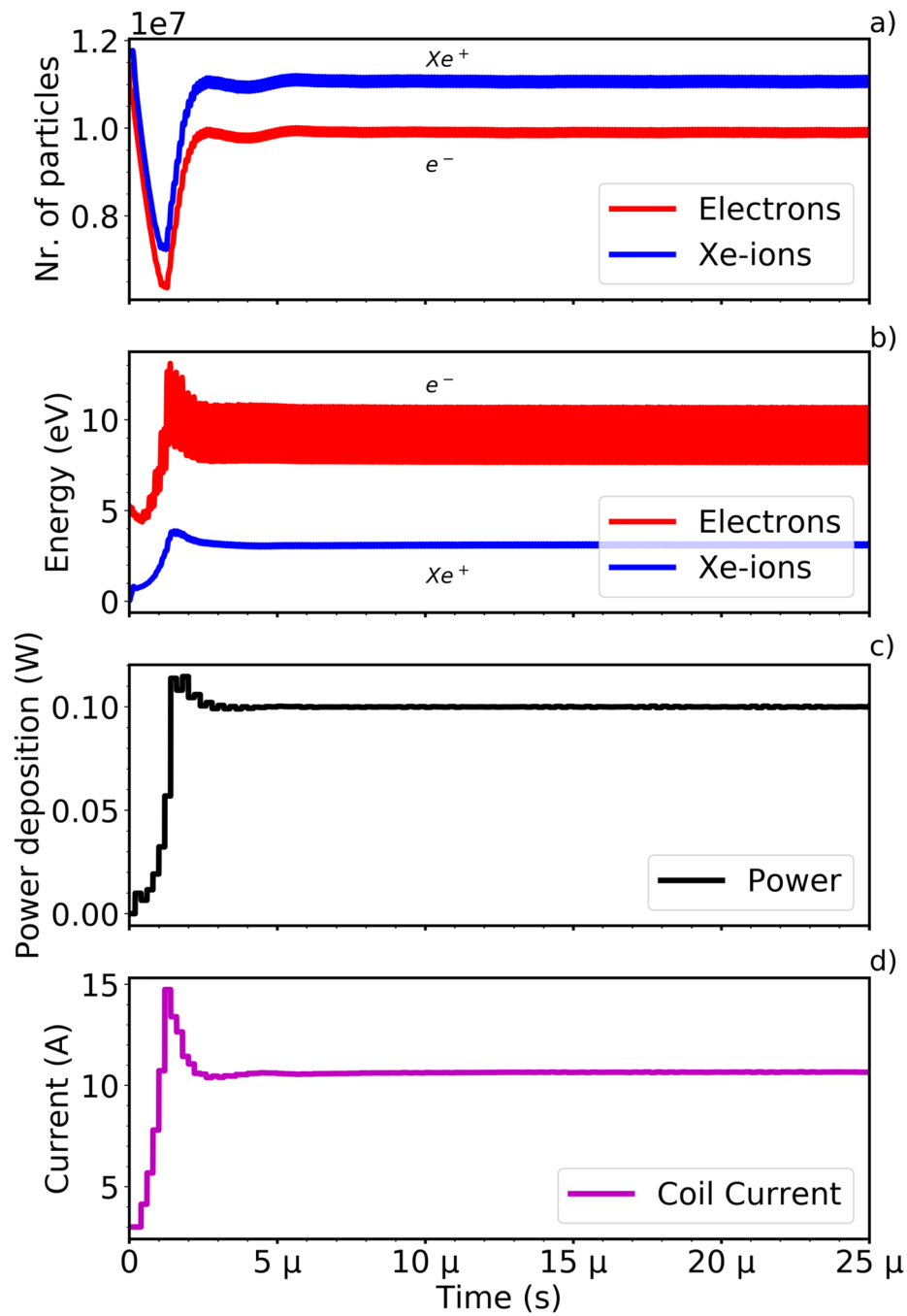
Fig. 4 The temporal evolution of (**a**) total number of particles in the plasma, (**b**) the mean energy of electrons and ions, (**c**) the power deposition and (**d**) the coil current for the entire simulation run showing the stable plasma generation after initial variations. (colour on-line)

measured using a Langmuir probe. For higher pressures, the plasma density is at its highest value in the middle of the discharge chamber and decreases towards the wall. In contrast, for lower pressure values the maximum of the plasma density is located at around half of the discharge chamber radius, and a drop of the density towards the middle of the discharge chamber is observed. Figure 8a shows ion densities simulated using
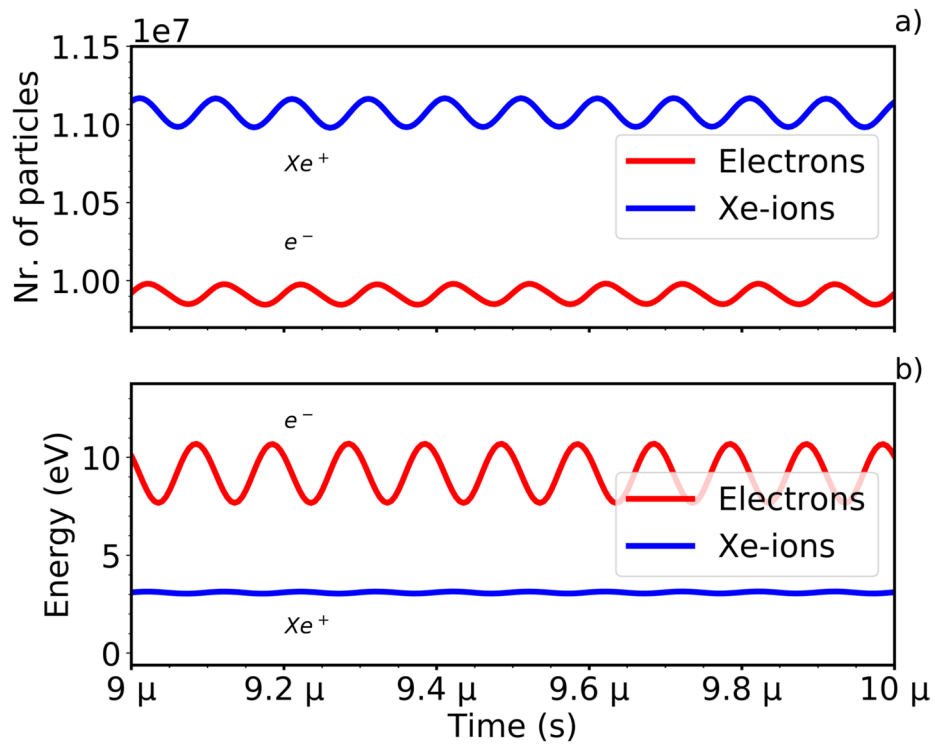
Fig. 5 The enlarged view showing the oscillatory behaviour in (**a**) the number of particles and (**b**) the energy after achieving stable plasma condition. (colour on-line)
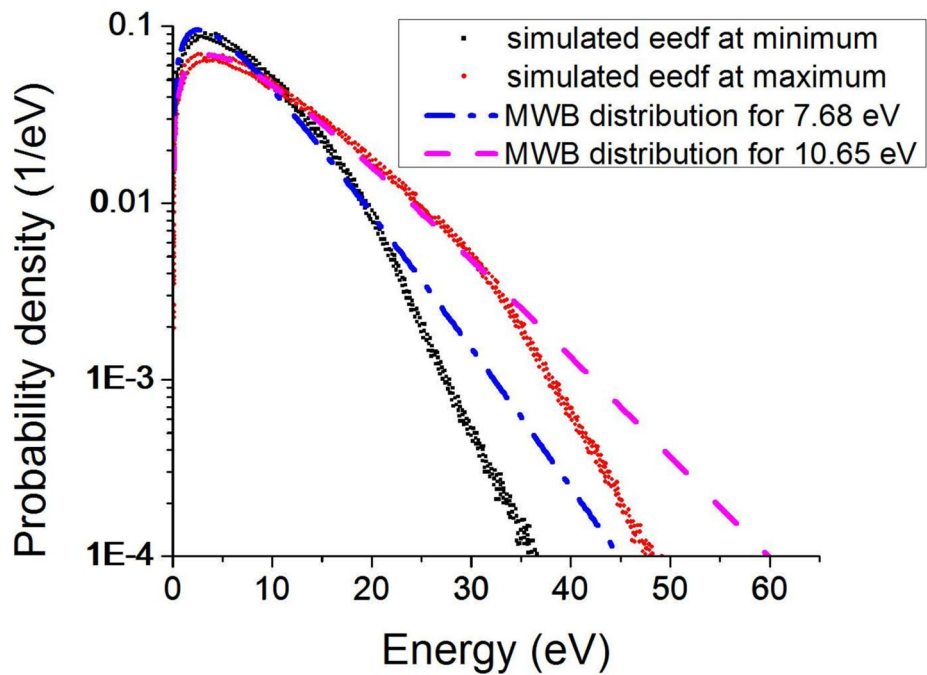

Fig. 6 The probability density function plotted as a function of electron energies at the minimum and at the maximum point of the energy after achieving stable plasma. (colour on-line)
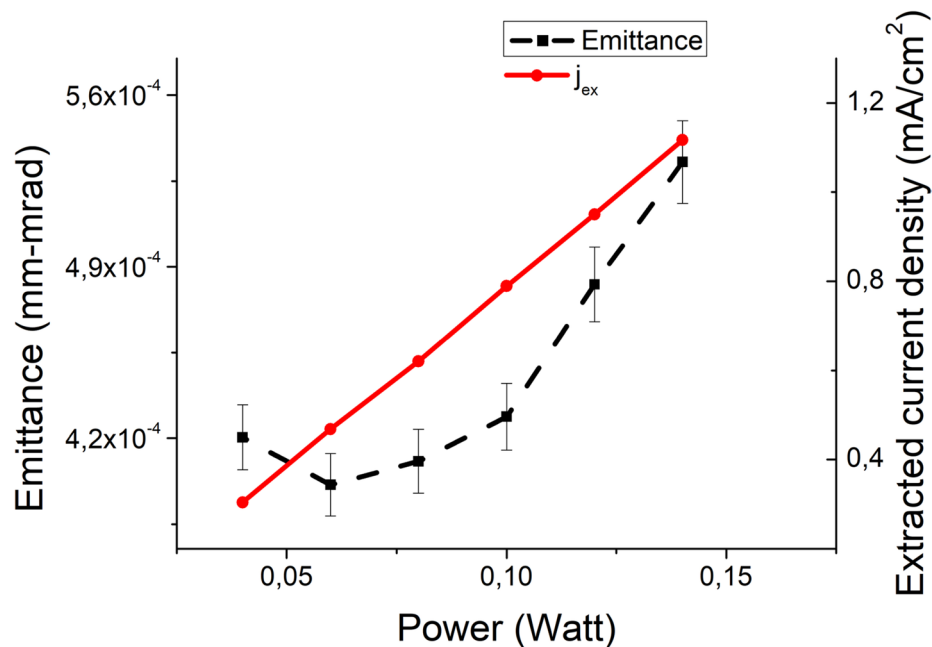
Fig. 7 Extracted current and transversal emittance growth as a function of power deposition. (colour on-line)

a neutral gas pressure of 0.35 Pa in RIT-1.0 which corresponds to a neutral gas pressure of 3.5×10^{-2} Pa in a RIT-10 according to scaling laws [28]. Similarly, Fig. 8b shows ion densities simulated using the neutral gas pressure of 4.1 Pa in RIT-1.0, which is comparable to values of about 4.1×10^{-1} Pa in RIT-10. For both simulations a power deposition of 0.06 W was applied. Hence, the shape of the simulated plasma density distribution qualitatively fits the measured values. The quantitative variation arises from the different power values applied. The characteristics of the ion density distribution correspond to the ones measured in Fig. 8c. By that it is demonstrated that the plasma density distribution in a RIT-1.0 shows a similar dependence on the neutral gas pressure as the one in a RIT-10.

Sensitivity of the design

The density distribution of the electrons in the discharge chamber is observed to be similar to the profile followed by ions. Both species show an asymmetry in the form of a one-sided dense torus due to coil slope and its varying radius (see Fig. 3). We show in Fig. 9a that, by substituting the coil with five single loops, the ion density distribution becomes rotationally symmetric. The left variation in the torus-shaped high ion density results from a slight shift of the coil against the discharge chamber. Figure 9b shows that when the coil is moved backwards (negative y-axis) by 0.3 mm, the ion density distribution breaks the symmetry showing its sensitive nature and a strong influence on the density profile from the geometry.

It has direct consequences observed on the beam quality. As seen in Fig. 10 the beam emittance increases by about 17% when the coil is moved and consequently plasma is off-centred.
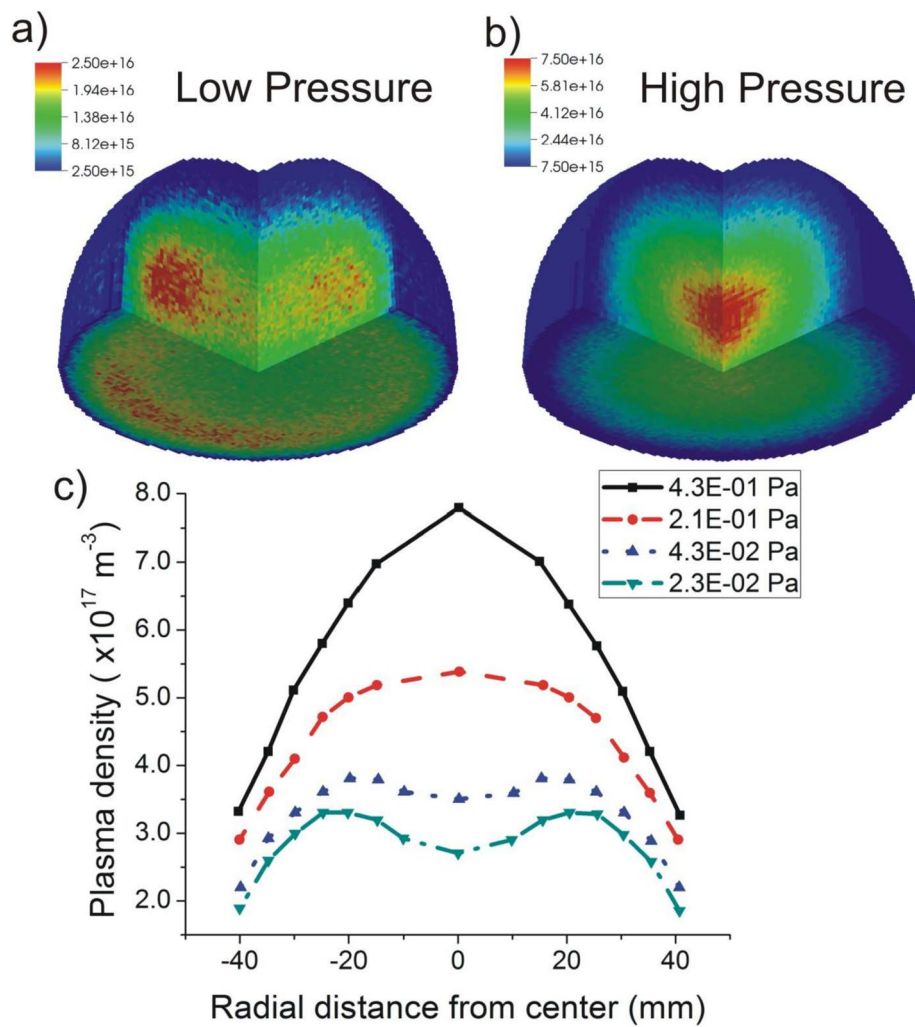
Fig. 8 Simulated ion densities in RIT-1.0 at (**a**) low pressure (0.35 Pa) and at (**b**) high pressure. (4.1 Pa).
(**c**) Experimental results for a RIT-10 showing qualitatively similar behaviour [27]. Note that the measurement
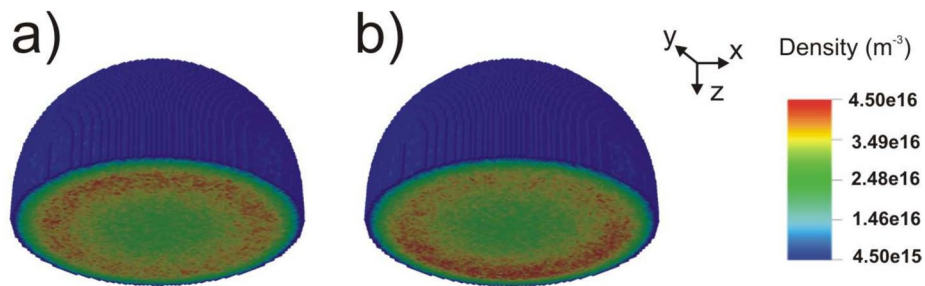was done only in one direction and symmetrized afterwards for better visualization. (colour on-line)

Fig. 9 a Ion density distribution for five single loops that are rotationally symmetric whereas, **b** the coil is
shifted backwards (negative y-axis) by 0.3 mm. (colour on-line)

Conclusion

In this framework, *PlasmaPIC*, a particle in cell code was employed for investigation
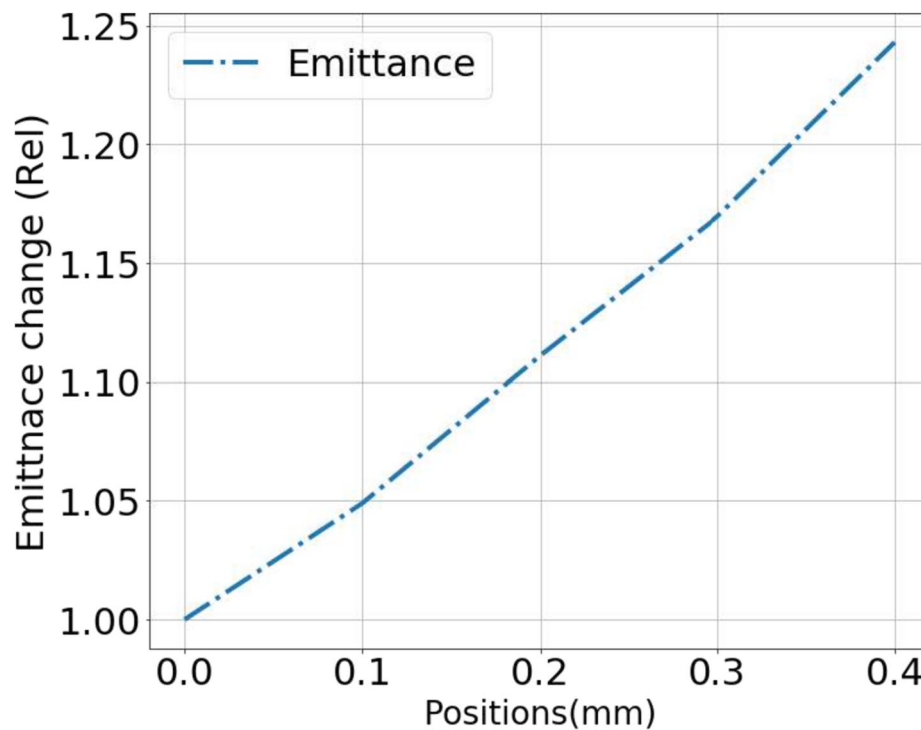of the plasma evolution and its properties inside a small-sized radio-frequency ion

Fig. 10 The emittance growth caused by radial shifting of ion distribution. (colour on-line)

thruster. RIT-1.0 thruster is a scaled down version of ion thruster family under consideration for ultra-fine positioning of the spacecrafts. Here, we have employed this code to investigate the working and feasibility of the RIT-1.0 thruster. The simulations showed that although the ion extraction is possible, RIT1.0 can be very sensitive to geometry and input parameters. The feasibility of such a device remains questionable as it requires more studies on structural integrity. On the other hand, the *PlasmaPIC* code has demonstrated its capabilities and usability in simulating small plasma devices. This open source code can be obtained on request and used for applications not just for ion thrusters but also ion sources and ion material interaction studies.

Authors' contributions
N. Joshi wrote the main manuscript text. N. Joshi and C. Heiliger reviewed the manuscript.

Availability of data and materials
Data sets generated during the current study are available from the corresponding author on reasonable request.

Declarations

Competing interests
The authors declare no competing interests.

References

1. Holste K (2020) Ion thrusters for electric propulsion: Scientific issues developing a niche technology into a game changer. Rev Sci Instrum 91(061101):1–55. https://doi.org/10.1063/5.0010134
2. Kanev S, Khartov S, Nigmatzyanov V (2017) Analytical model of radio-frequency ion thruster. Procedia Eng 185:31–38
3. Leiter H et al (2002) Evaluation of the performance of the advanced 200mn radio-frequency ion thruster rit-xt. In: Proceedings of 38th AIAA-ASME-SAE-ASEE Joint Propulsion Conference and Exhibit. American Institute of Aeronautics and Astronautics, Inc. https://doi.org/10.2514/6.2002-3836
4. Killinger R et al (2000) Rit a ion propulsion for artemis lifetime test results. In: Proceedings of 36th AIAA-ASME-SAE-ASEE Joint Propulsion Conference and Exhibit. American Institute of Aeronautics and Astronautics, Reston
5. Samples SA, Wirz RE (2019) Development status of the miniature xenon ion thruster. In: Proceedings of 36th International Electric Propulsion Conference (IEPC-2019-143), University of Vienna, Vienna, 15–20 September 2019
6. Yang X et al (2022) Numerical simulation of the start-up process of a miniature ion thruster. Plasma Sci Technol 24(7):074007. https://doi.org/10.1088/2058-6272/ac5ee7
7. KOIZUMI H, KOMURASAKI K, AOYAMA J, YAMAGUCHI K (2014) Engineering model of the miniature ion propulsion system for the nano-satellite: Hodoyoshi-4. Trans JSASS Aerosp Tech Jpn 12(ists29):Tb_19–Tb_24
8. Hey F et al (2013) Development of a highly precise micro-newton thrust balance. In: 33rd International Electric Propulsion Conference IEPC-2013-275. IEEE, New York
9. Rock B, Blandino J, Demetriou M (2004) Application of micronewton thrusters for control of multispacecraft formations in earth orbit. In: Proceedings of 40th AIAA-ASME-SAE-ASEE Joint Propulsion Conference and Exhibit AIAA 2004-3811. American Institute of Aeronautics and Astronautics, Reston
10. Lie T, Kurniawan H, Hedwig R, Pardede M (2005) Low pressure plasma confined in a miniature cylindrical chamber and its application for in-situ elemental analysis. Jpn J Appl Phys 44(1A):202–209
11. Verboncoeur J, Langdon A, Gladd N (1995) An object-oriented electromagnetic pic code. Comput Phys Commun 87:199–211
12. Henrich R, Heiliger C (2012) Neutral gas and plasma simulation. Internal publication of Workshop RITSAT summer school Physik im Weltraum, Usedom
13. Hockney RW, Eastwood JW (1981) Computer simulation using particles. McGraw-Hill, New York
14. Birdsall CK, Langdon AB (1985) Plasma physics via computer simulation. McGraw-Hil, New York
15. Birdsall CK (1991) Particle-in cell charged-particle simulations, plus monte carlo collisions with neutral atoms, pic-mcc. IEEE Trans Plasma Sci 19:65–85
16. Vahedi V, M. Surendra M (1995) A monte carlo collision model for the particle-in-cell method: applications to argon and oxygen discharges. Comput Phys Commun 87:179–198
17. Yu BW, Girshick SL (1991) Modeling inductively coupled plasmas: The coil current boundary condition. J Appl Phys 69(2):656–661
18. You KI, Yoon NS (1999) Discharge impedance of solenoidal inductively coupled plasma discharge. Phys Rev E 59:7074–7084
19. Takao Y, Kusaba N, Eriguchi K, Ono K (2010) Two- dimensional particle-in-cell monte carlo simulation of a miniature inductively coupled plasma source. J Appl Phys 108(9):093309
20. Henrich R, Heiliger C (2013) Three dimensional simulation of micro newton rits. In: Proceedings of 33rd International Electric Propulsion Conference, The George Washington University, Washington, 6–10 October 2013
21. Young D (1950) Iterative methods for solving partial difference equations of elliptical type. PhD thesis, Harvard University
22. Boris J (1970) Relativistic plasma simulation-optimization of a hybrid code. In: Proceedings of the 4th Conference on Numerical Simulation of Plasmas Naval Res Lab. pp 3–67
23. Bird G (1994) Molecular gas dynamics and the direct simulation of gas flows. Oxford Science Publications, Oxford
24. White C, Borg M, Scanlon T, Longshaw S, John B, Emerson D (2018) dsmcfoam+: An openfoam based direct simulation monte carlo. Comput Phys Commun 224:22–43
25. Abe T (1993) dsmcfoam+: An openfoam based direct simulation monte carlo. Comput Fluids 22:253–257
26. Henrich R (2009) Entwicklung eines simulationsprogramms zur bestimmung des dichteprofils bei molekularer stroemung. PhD thesis, Justus-Liebig-Universitaet Giessen
27. Schaefer M (1971) Plasmadiagnostik und energiebilanzunterscuhung an dem hf-ionentriebwerk rit-10. PhD thesis, Justus-Liebig-Universitaet Giessen
28. Loeb H, Schartner KH, Weis S, Feili D, Meyer B () Development of rit- microthrusters. In: Proceedings of 55th International Astronautical Congress of the International Astronautical Federation, the International Academy of Astronautics, and the International Institute of Space Law, 04 October 2004 - 08 October 2004. Vancouver. https://doi.org/10.2514/6.IAC-04-S.4.04

Publisher's Note